

PulseNet: Deep Learning ecg-signal classification using random augmentation policy and continuous wavelet transform for canines

Andre Dourson¹, Roberto Santilli^{3,5}, Federica Marchesotti³, Jennifer Schneiderman⁴,
Oliver Roman Stiel², Fernando Junior¹, Michael Fitzke¹, Norbert Sithirangathan¹,
Emil Wallerer¹, Xiaoli Qiao¹, Mark Parkinson¹

¹Mars Digital Technologies

² Mars Petcare

³Anicura

⁴Antech Imaging Services

⁵Cornell University

May 16, 2023

Abstract

Evaluating canine electrocardiograms (ECG) require skilled veterinarians, but current availability of veterinary cardiologists for ECG interpretation and diagnostic support is limited. Developing tools for automated assessment of ECG sequences can improve veterinary care by providing clinicians real-time results and decision support tools. We implement a deep convolutional neural network (CNN) approach for classifying canine electrocardiogram sequences as either normal or abnormal. ECG records are converted into 8 second Lead II sequences and classified as either normal (no evidence of cardiac abnormalities) or abnormal (presence of one or more cardiac abnormalities). For training ECG sequences are randomly augmented using RandomAugmentECG, a new augmentation library implemented specifically for this project. Each chunk is then converted using a continuous wavelet transform into a 2D scalogram. The 2D scalogram are then classified as either normal or abnormal by a binary CNN classifier. Experimental results are validated against three boarded veterinary cardiologists achieving an AUC-ROC score of 0.9506 on test dataset matching human level performance. Additionally, we describe model deployment to Microsoft Azure using an MLOps approach. To our knowledge, this work is one of the first attempts to implement a deep learning model to automatically classify ECG sequences for canines. Implementing automated ECG classification will enhance veterinary care through improved diagnostic performance and increased clinic efficiency.

1 Introduction

The role of electrocardiography (ECG) in the veterinary diagnostic work-up had increased in the last decades becoming an important tool to diagnose different primary and secondary rhythm disturbances such as atrial fibrillation, focal atrial tachycardias, junctional tachycardias, reciprocating tachycardias, atrial flutter, and ventricular arrhythmias and conduction abnormalities. [1][2][3][4][5][6][7][8][9][10][11][12][13] The analysis of ECG appearance is complex and diagnosis of specific arrhythmias often requires veterinary cardiologist review. However, the shortage of trained veterinary specialists makes this challenging.[14]

Electrocardiogram (ECG) shows cardiac electrical activities, named vectors, projected on the body surface allowing the analysis of cardiac arrhythmias, ischemia, and conduction abnormalities.[15]

The cardiac vectors can be analyzed on the frontal plane using the 6 lead system (I,II,III, aVR, aVL, aVF) and on the horizontal plane using the precordial system (V1,V2,V3,V4, V5, V6) modified for the dog. [15] [16]. They appear as consecutive waves (atrial – P wave and ventricular – QRS complex) displayed on a millimeter paper at different programmed speed and calibration.[15]

For this reason, with the help of artificial intelligence (AI) the interpretation process can be speed up, differentiating first normal from abnormal electrocardiogram and then grouping them in several subgroups of arrhythmias then submitted to the cardiologists for a final diagnosis.

2 Related Work

The problem of automated ECG classification is well-studied in the field of human medicine, and numerous deep learning models have been proposed to tackle this task ([17][18] [19]). However, the problem of automated ECG classification for canines has received limited attention in the literature, and few deep learning models have been proposed for this specific purpose. Previous work with automated classification of canine ECG signals has focused on extracting ECG waveform details and applying a decision algorithm for categorizing abnormalities [20].

The current state-of-the-art in automated ECG classification for humans often relies on deep convolutional neural networks (CNNs) and various data augmentation techniques ([21], [22]). Our work builds upon these approaches by adapting them for canine ECG signal classification.

Our work shares similarities with the recent development of ECG-based deep learning models for other non-human animals, such as horses ([23]) and mice ([24]). These studies demonstrate the potential of leveraging deep learning approaches for animal ECG classification. Our study contributes to this emerging field by focusing on canines and exploring the impact of random augmentation policies and continuous wavelet transforms on classification performance.

Zero-shot transfer from humans to canines are discussed in [25] with results indicating that dedicated models trained on canine are needed to ensure reliable predictions. This work fills that gap by presenting a novel contribution to the field of automated ECG classification for canines. By incorporating state-of-the-art techniques from human ECG analysis and introducing new methods specifically tailored for canine ECG signals, we demonstrate the potential of deep learning models to improve diagnostic performance and clinical efficiency in veterinary medicine.

3 Data

3.1 DICOM files

The ECG records used in this project were collected from 1462 distinct DICOM files, containing 6 or 12 leads and all sampled at 500Hz. For this project we utilized only lead II, which has shown comparable performance to inclusion of additional leads [26].

The collected ECG raw sequences have various durations (Figure 1) :

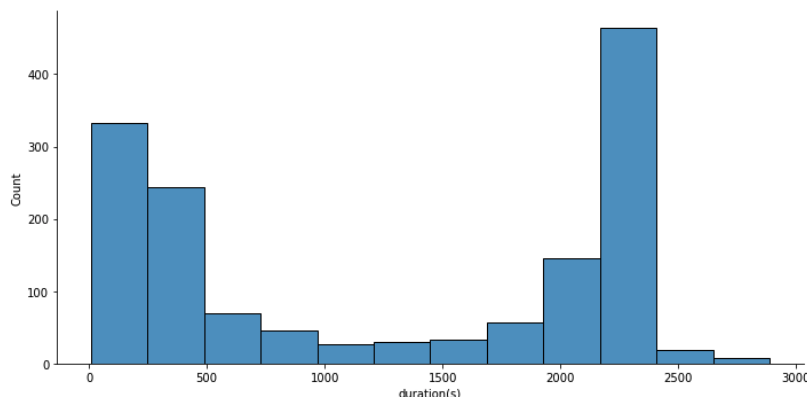


Figure 1: Distribution of ECG sequence length (in seconds)

In order to prepare our dataset for training, the ecg signals were extracted from DICOM format into one dimensional arrays. The extracted signals were then pre-processed using the following pipeline (Figure 2) :

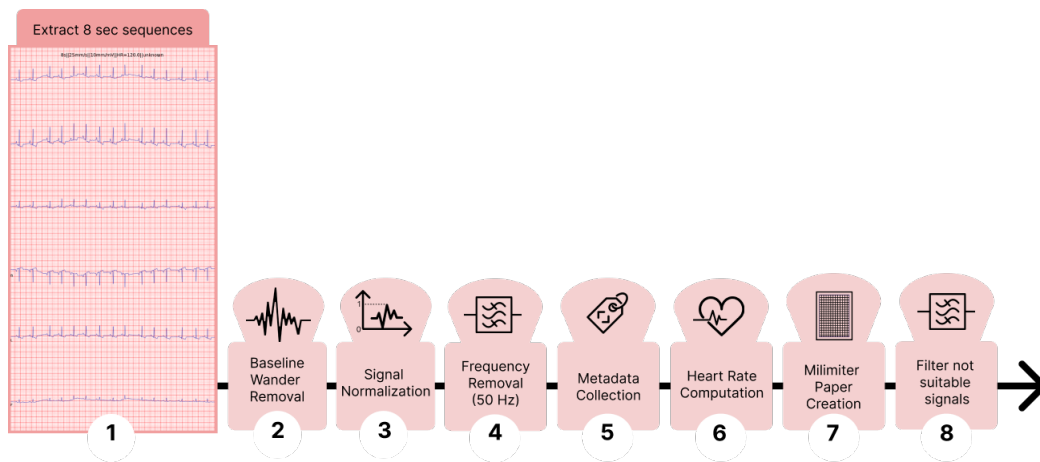


Figure 2: Pre-processing steps

- (1) Extraction of 8 seconds sequences with an overlap of 1 second between each sequence
- (2) Baseline wander removal
- (3) Signal normalization between 0 and 1
- (4) Frequency removal (50Hz)
- (5) Collection of metadata (race, breed, age, weight etc...)
- (6) Automatic computation of the heart rate
- (7) Creation of (millimeter paper look and feel) 8 seconds snippets for experts review
- (8) Removal of signals which are not suitable for diagnostics

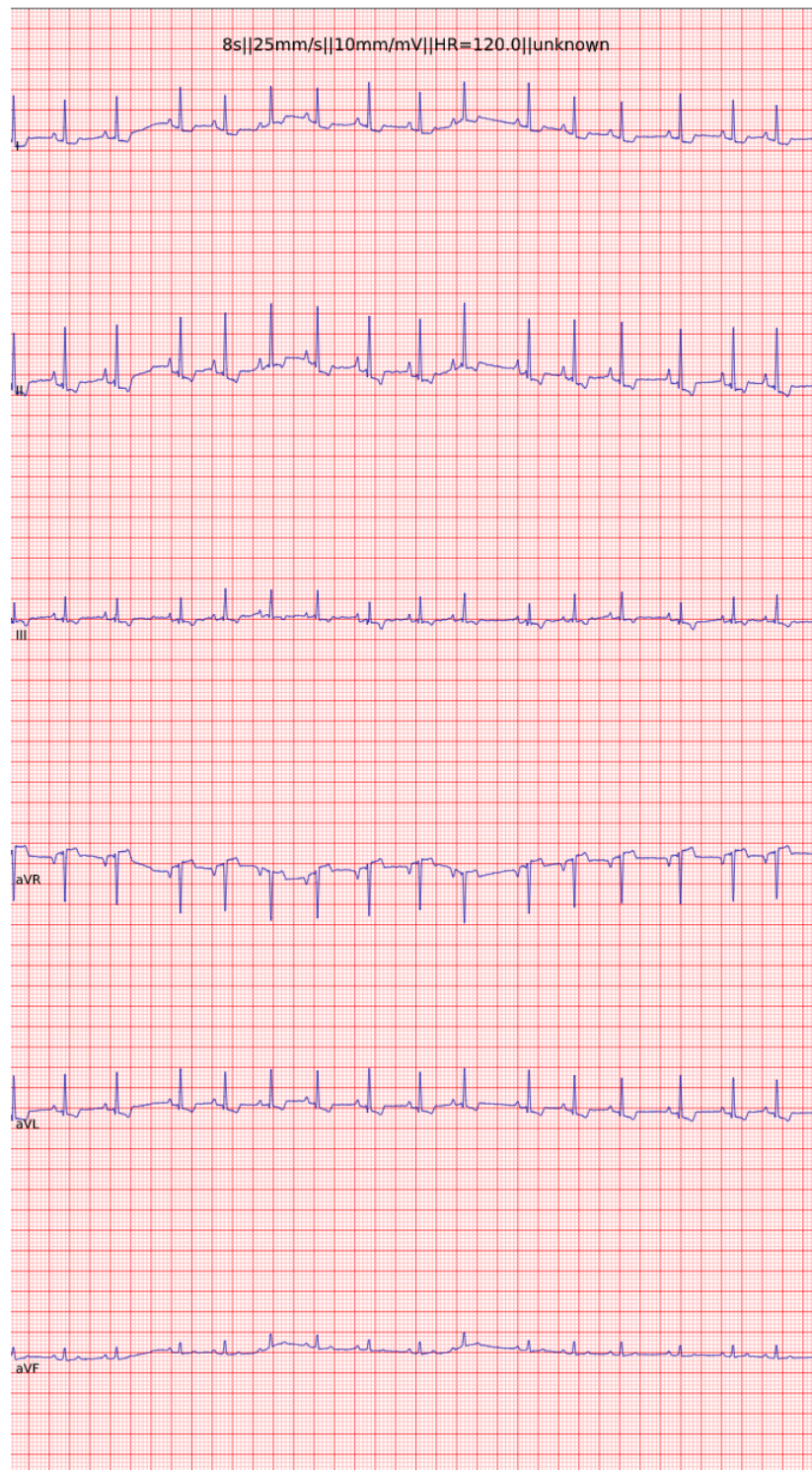


Figure 3: Example of 8 seconds snippet

We extracted a total of 222,847 sequences of 8 seconds (Lead II signal) following the previously described steps (Figure 3). These 8 seconds signal chunks were then categorized into seven categories (normal, unsuitable for diagnosis, supraventricular arrhythmias, ventricular arrhythmias, bradyarrhythmias, and conduction disorders) by veterinary board certified cardiologists. (Figure 4). Unsuitable for diagnostic chunks were removed from the dataset, and all arrhythmias were then grouped into a single abnormal category.

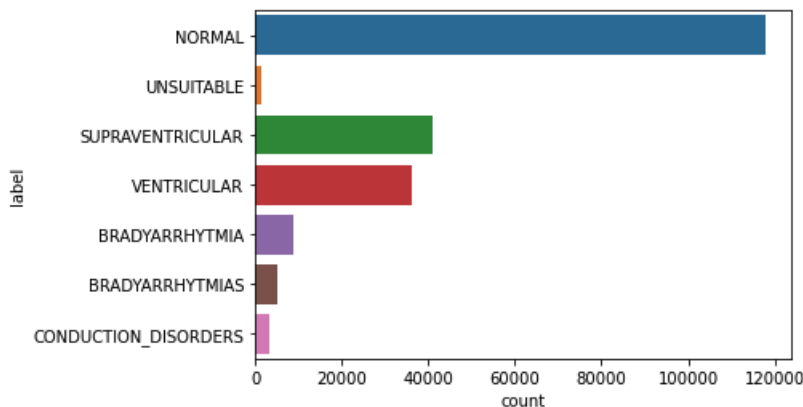


Figure 4: ECG sequences labels

3.2 RandAugmentECG library

Data augmentation of image data is a key strategy to improve neural network performance [27]. Similar performance improvements may be possible for one-dimensional data, like ECG segments. In this paper we introduce RandAugmentECG, a PyTorch ECG augmentation library inspired from the work done by [28] and [29] and a one-dimensional equivalent to the library developed for images [30].

This PyTorch library provides custom augmentation listed below :

- RandShift1d : randomly shifts a portion of the signal
- RandScale1d : randomly scales the signal by a given factor
- RandRoll1d : rolls one random portion of the signal
- RandDrop1d : randomly drops one consecutive portion of the signal, replacing with a specific number (zero for instance)
- RandAddSine1d : adds a randomly generated sinusoidal signal to the source signal
- RandAddSinePartial1d : adds a randomly generated sinusoidal signal to a random consecutive portion of the source signal
- RandAddSquarePulse1d : adds a random pulse square signal to the source signal
- RandAddSquarePulsePartial1d : adds a random pulse square signal to a random consecutive portion of the source signal
- RandAddGaussianNoise1d : adds a random gaussian noise to the source signal
- ToTensor1d : converts source signal to 1D tensor
- Resample1d : resamples the source signal to given frequency
- Normalize1d : normalizes the source signal between 0 and 1
- Standardize1d : standardizes the source signal
- ZeroPad1d: if the signal is shorter than the expected length, pads the signal with zeros
- FillEmpty1d : if the signal contains NaN elements, replaces these elements with zeros
- RemoveBaselineWander1d : removes signal wander line
- RemoveFrequency1d : removes a given frequency from the signal
- ToCWT : converts the 1D signal to a 2D scalogram (continuous wavelet transform)

- ToSTFT : converts the 1D signal to a 2D spectrogram (Short time Fourier Transform)
- ToCWFT : converts the 1D signal a mix of CWT and STFT (either summing up or concatenating)

The purpose of RandAugmentECG is similar to the work done by for 1D signal and for 2D images. It consists on applying a stochastic combination of several 1 dimensional transforms present in the library :

- RandShift1d
- RandScale1d
- RandRoll1d
- RandDrop1d
- RandAddSine1d
- RandAddSquarePulse1d
- RandAddGaussianNoise1d

The maximum number of individual transforms to be applied along with the magnitude of the change are governed by two parameters n and m (Figure 5)

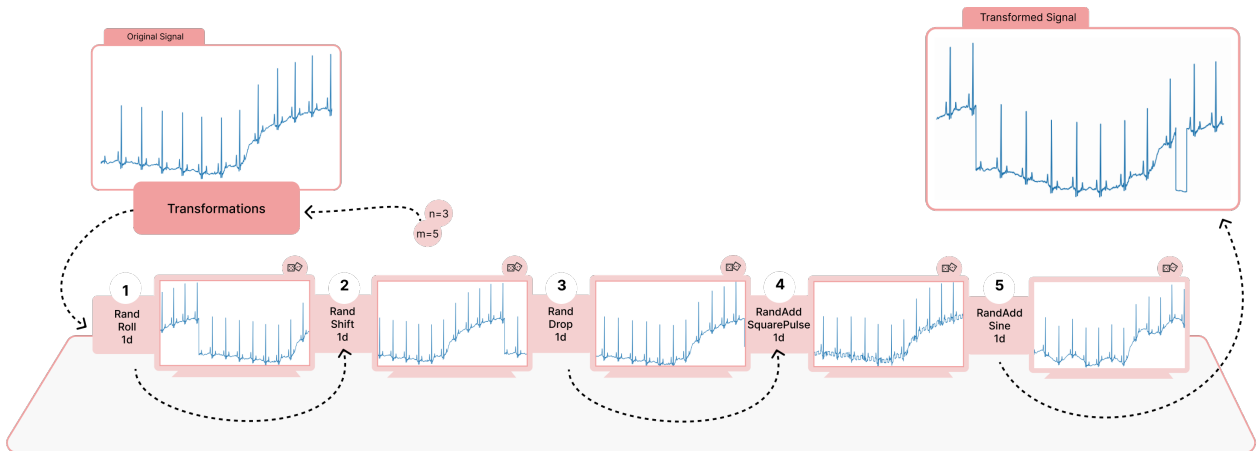


Figure 5: RandAugmentECG samples ($n=3,m=5$)

3.3 Continuous Wavelet transform

Wavelet transform[31][32] and Short Time Fourier transform[33] are widely used in signal processing applications. As opposed to Fourier transform where we analyse the time/frequency domain for a window (portion) of the signal and then do a sliding of this window to reiterate the same analysis before eventually recombining all resulting transforms, Continuous Wavelet transform has the benefit to be able to process the entirety of the signal at once, modulating the wavelet dilation and location, and doing a convolution between the resulting wavelet function and the signal (Figure 6).

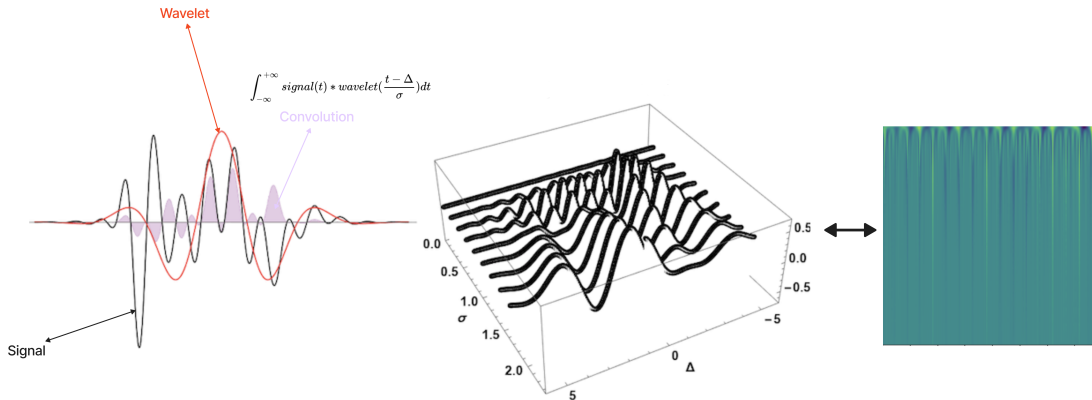


Figure 6: convolution of wavelets with input signal to render the scalogram

If $x(t)$ is a continuous signal, at a scale $\sigma > 0$, $\sigma \in \mathbb{R}^{+*}$, $\Delta \in \mathbb{R}$ then its wavelet transform is defined as

$$X_w(\sigma, \Delta) = \frac{1}{|\sigma|^{1/2}} \int_{-\infty}^{+\infty} x(t) \bar{\psi}\left(\frac{t-\Delta}{\sigma}\right) dt$$

where $\psi(t)$ is a continuous function in both the time domain and the frequency domain called the mother wavelet, and $\bar{\psi}$ is its complex conjugate. σ is also called the dilation parameter of the wavelet and Δ is called the location parameter of the wavelet

The purpose of the mother wavelet is to provide a new version of it called the daughter wavelet, which is a translated and scaled version of the mother wavelet (defined by the σ and δ parameters).

For ECG, a particular type of wavelet seems intuitively to be appropriate (as it somewhat mimics the ECG shape): the Ricker wavelet, a.k.a. Mexican hat wavelet (due to its shape of a sombrero). The Mexican hat wavelet (Figure 7) is defined as the second derivative of a Gaussian function given by

$$\psi(t) = \frac{2}{\sqrt{3}\sigma\pi^4} \left(1 - \left(\frac{t}{\sigma}\right)^2\right) e^{-\frac{t}{2\sigma^2}}$$

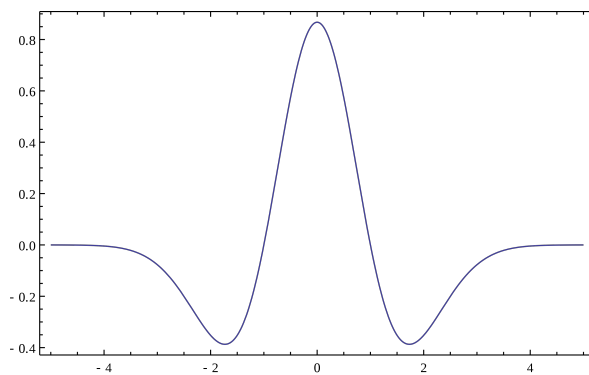


Figure 7: Ricker wavelet a.k.a. Mexican hat wavelet

3.4 Creation of training dataset

We split the 222,847 ECG records into a training and a validation dataset (99%/1%). On the training set, we first applied the Resample1d transform to resample each signal to 250Hz in order to reduce the computation cost. Next, we further transformed the signals by stochastically augmenting each signal using the RandAugmentECG transform ($n=5$, $m=5$). We finally converted the augmented signals using the ToCWT transform into a 2D scalogram of size 300x300 (Figure 8).

On the validation set, we only applied the Resample1d transform to resample signals to 250Hz to remain consistent with our training dataset.

Using this approach we are in turn converting this task into a more standard image classification problem.

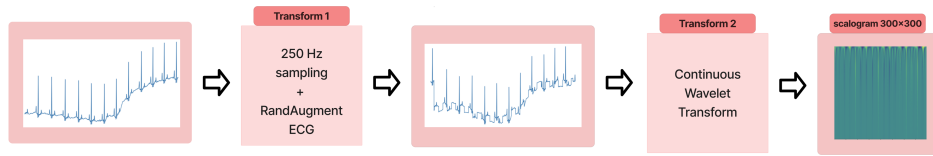


Figure 8: scalogram creation

4 Models and training details

4.1 Model Architecture

We initially trained our model using standard types of convolutional neural networks architecture (ResNet18, ResNet34, ResNet50) but we also designed our own architectures. One custom architecture, named "R" model (Figure 10 and Table 2), was inspired by the ResNet architecture [34] but with only 3 ResNet blocks, and with the replacement of Max Pooling with Average Pooling[35]. The second architecture, designated type "M" (Figure 9 and Table 3) is composed of 3 layers, each consisting of a 2D convolutional layer followed by Batch Normalization, ReLU activation and Average pooling. Both "M" and "R" models are implemented with Dropout in the final classification layer ($p = 0.2$). From our experiments, the best performance as determined by area under the receiver operating characteristic curve (AUC) were achieved using the "M" architecture, followed closely by "R" architecture.

The intuition behind replacement of Max Pooling with Average Pooling in our models could be that Average Pooling would be more likely be to extract useful features from scalograms as transition/edges are less abrupt in scalograms vs regular images (where contours are maybe more apparent). (Table 1)

Max AUC per model architecture	
Architecture	Max AUC
Resnet18	0.906
Resnet34	0.922
Resnet50	0.922
"R" model	0.941
"M" model	0.951

Table 1: Models architecture : comparison of AUC value

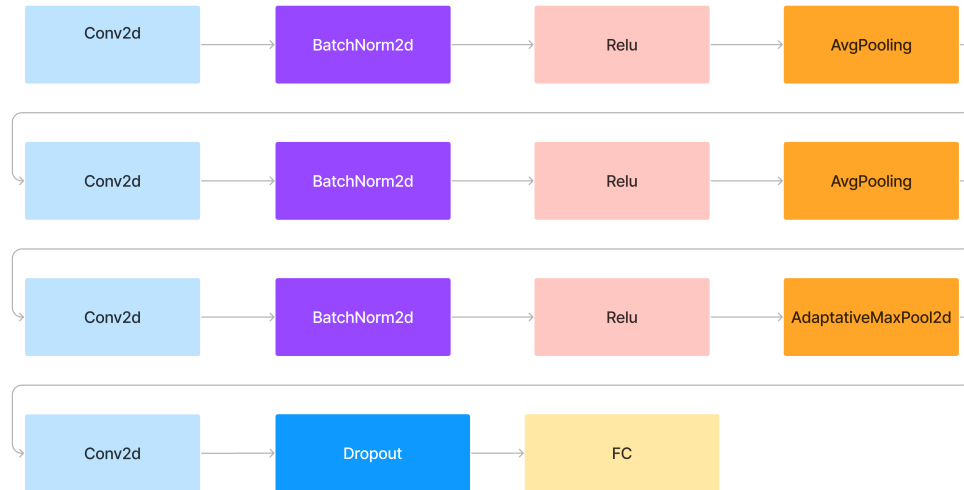


Figure 9: "M" model

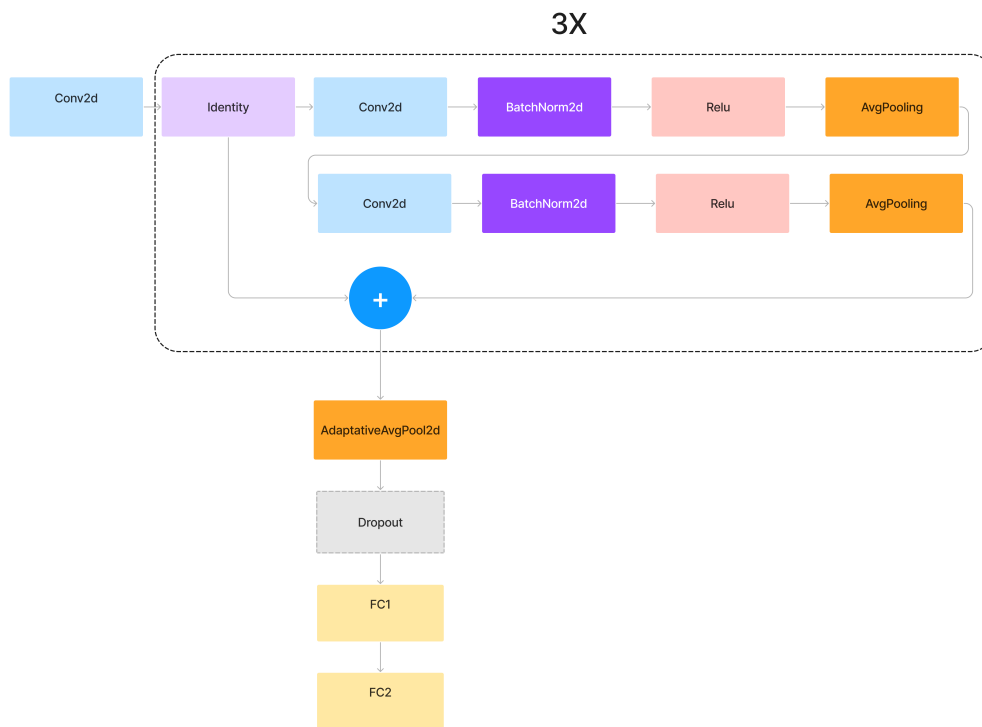


Figure 10: "R" model

Architecture of "R" Model						
Layer	Type	Kernel size	Stride	Padding	Features	Input size
Layer1	Conv2d	7 x 7	2	3	64	1 x 300 x 300
Layer2	Conv2d	3 x 3	1	1	32	1 x 300 x 300
Layer3	Conv2d	3 x 3	1	1	64	32 x 300 x 300
Layer4	AvgPool2d	2 x 2	2	0	-	64 x 300 x 300
Layer5	Conv2d	3 x 3	1	1	128	64 x 150 x 150
Layer6	Conv2d	3 x 3	1	1	256	128 x 150 x 150
Layer7	AvgPool2d	2 x 2	2	0	-	256 x 152 x 152
Layer8	Conv2d	3 x 3	1	1	512	256 x 76 x 76
Layer9	Conv2d	3 x 3	1	1	1024	512 x 76 x 76
Layer10	AvgPool2d	2 x 2	2	0	-	1024 x 76 x 76
Layer11	AdpAvP2d	-	-	-	1024	1024 x 38 x 38
Layer12	Linear				256	1024 x 1 x 1
Layer13	Linear				2	256

Table 2: Architecture of "R" model

Architecture of "M" Model						
Layer	Type	Kernel size	Stride	Padding	Features	Input size
Layer1	Conv2d	7 x 7	1	0	128	1 x 300 x 300
Layer2	AvgPool2d	5 x 5	2	0	-	128 x 294 x 294
Layer3	Conv2d	3 x 3	1	0	256	128 x 58 x 58
Layer4	AvgPool2d	3 x 3	2	0	-	256 x 56 x 56
Layer5	Conv2d	3 x 3	1	0	512	256 x 18 x 18
Layer6	AdMaxP2d	-	-	-	512	512 x 16 x 16
Layer7	Conv2d	1 x 1	1	0	512	512 x 1 x 1
Layer8	Linear	-	-	-	2	512

Table 3: Architecture of "M" model

4.2 Training details

In all our experiments, we used PyTorch Lightning [36] to train and evaluate our models. The 2 models were each trained using a Tesla V100 system (16 Gb). We trained using mixed precision for 100 epochs with a batch size of 110 (for "M" model) and 80 (for "R" model), and we applied a gradient accumulation policy as optimization occurred only every 3 mini batches. Both models were initialized using Xavier initialization [37] and a Softmax activation was applied on the final layer. We used an Adam optimizer with a initial learning rate of 3e-4 with a weight decay of 0.2. The learning rate was

decayed using CosineAnnealing with warm restart (Figure 11), with the maximum learning rate of $3e-4$ and a τ^0 of 5000.

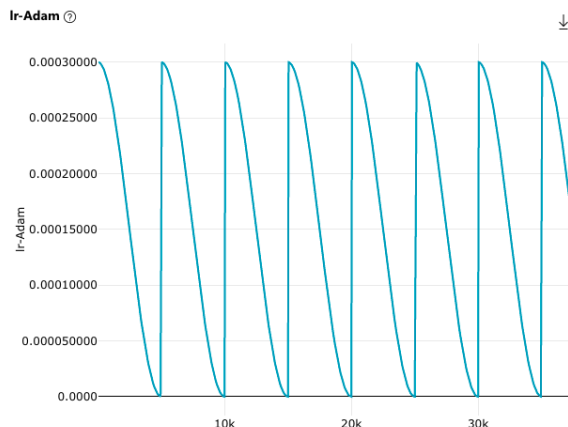


Figure 11: Cosine Annealing with warm restart

We trained the models using CrossEntropyLoss[38], but also with the PolyLoss described in[39]. Our experiments show the best results with PolyLoss (epsilon=2.5 or 3.5).

$$PolyLoss = - \sum_{n=1}^k y_i * \log(\hat{y}_i) + \epsilon * (1 - \hat{y}_i)$$

5 Testing

All testing was performed on a "gold" dataset containing 808 sequences of 8 seconds extracted from different DICOM files than the ones used to train and validate the model. These sequences were labeled independently by three board certified veterinary cardiologists. Gold standard or ground truth was determined using majority vote between the three cardiologist assessment (normal vs. abnormal). We benchmarked our best performing model (determined by AUC on our validation dataset), against human cardiologist performance. We then used our best model to benchmark it against the human expert using the ROC curve, using a threshold computed using Youden methodology to determine the ideal cutoff to distinguish between normal and abnormal classes. Our best model ("M" model) achieved an AUC score of 0.9506 and a F1 score (weighted) of 89,28%. Precision is 86,28% , Recall is 92,5%, Accuracy is 91,95%

Comparing with the cardiologists, the model is on par with 2 of them with respect to the F1 score, and doing better than 2 of them in term of Recall and Accuracy (Table 4, Figure 12 and Figure 13)

Comparison model vs cardiologists				
Metric	Model	Cardiologist0	Cardiologist1	Cardiologist2
F1	89,28%	88,37%	97,89%	89,85%
Precision	86,28%	98,46%	97,51%	95,11%
Recall	92,50%	80,15%	98,28%	85,15%
Accuracy	91,95%	83,63%	96,72%	85,09%

Table 4: Best Model vs Cardiologists

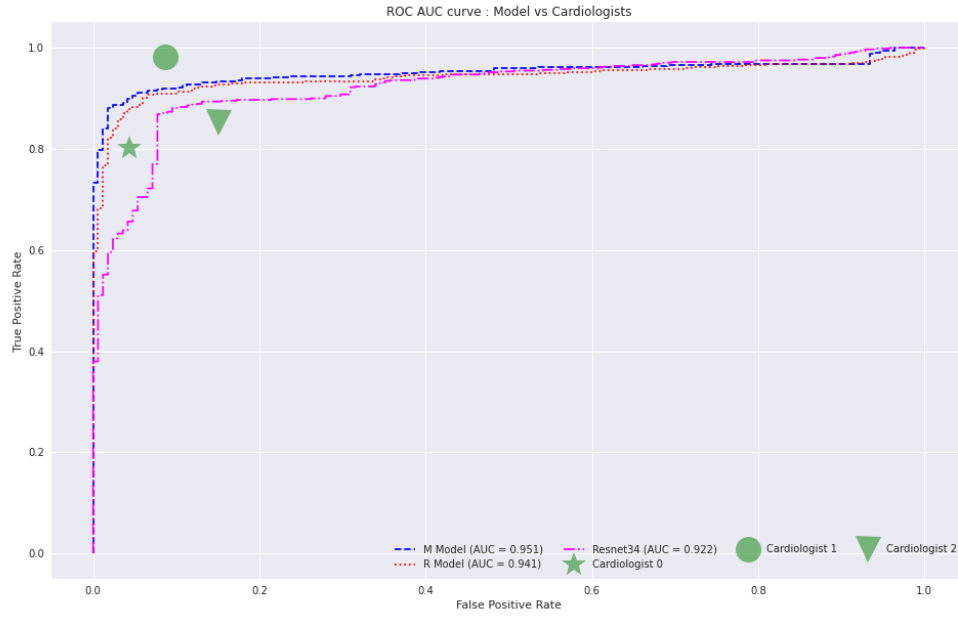


Figure 12: ROC curve : models vs cardiologists

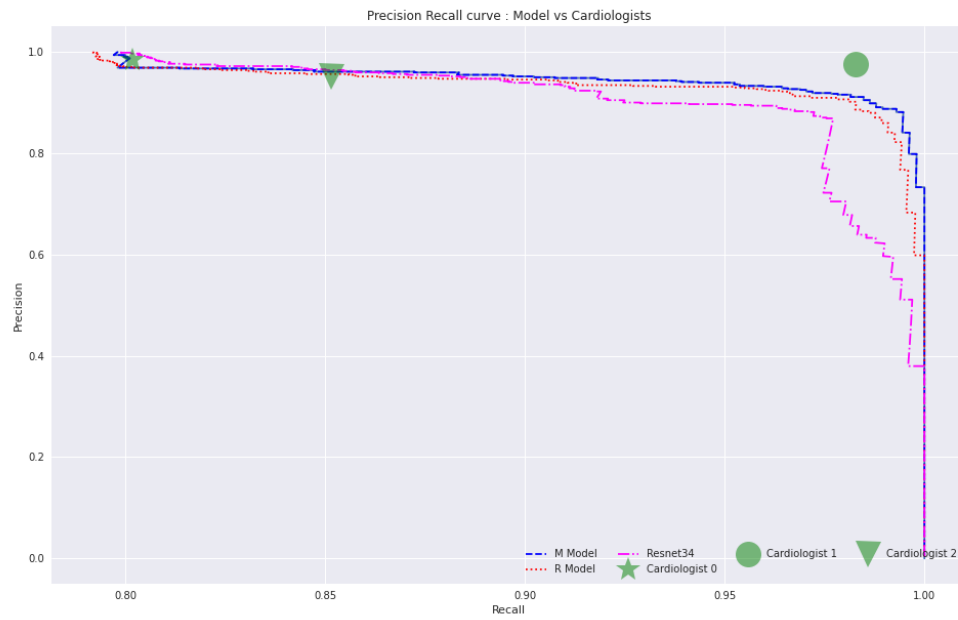


Figure 13: Precision Recall curve : models vs cardiologists

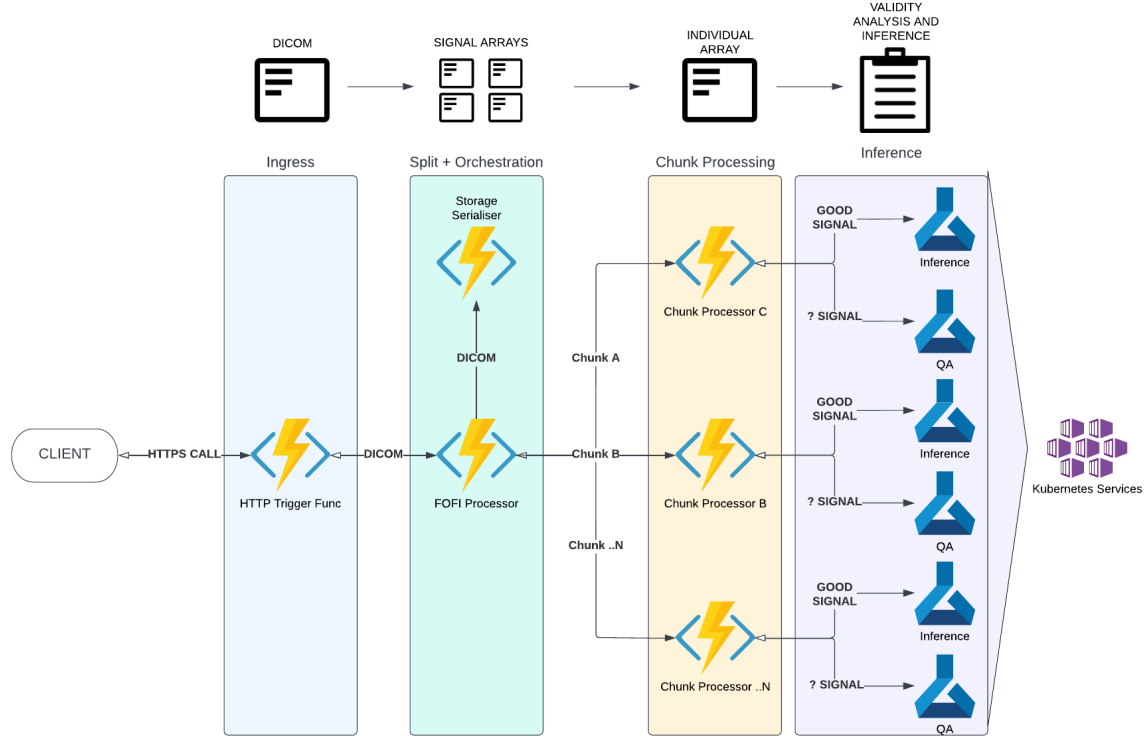


Figure 14: High level functional diagram

6 Deployment

For deployment of the system, we elected to follow a microservices-driven architecture, hosted in the Microsoft Azure Cloud across a collection of Azure services. Summarised, these services were:

DevOps Utilized for Git repositories, pipelines and build agents.

Function Apps Utilized as an HTTP middleware to facilitate communication between model endpoints and client applications.

Machine Learning Utilized for experimentation, log management, artifact management and as the interface for Azure Kubernetes-hosted model endpoints.

Kubernetes Service Utilized as the infrastructure layer for hosting of model endpoints.

Storage Accounts Utilized for storage of ingested signal data for the purposes of retraining and analysis.

Application Insights Utilized for application monitoring for both the Function App hosted middleware, and the Azure Kubernetes Service hosted model endpoints.

In this instance, inference is performed on a collection of independent 8 second sequences, with individual model responses then aggregated to a reported result over all sequences. As there is no need to communicate state between sequence instances, or for these sequences to be executed consecutively, it can be considered an "embarrassingly parallel" problem. For this problem, we elected to use the "Durable Functions" extension of Azure Function Apps. Durable Functions allows for the creation of more nuanced orchestrations of computation, while maintaining the inherent scalability and fault tolerance of a normal Function App, which are important for the usability of the solution.

In pseudocode, this orchestration can be seen as:

```

array_of_signals = transform_input_signal_into_chunk_array(input_signal)

array_of_tasks = [empty array]

for each chunk in array_of_signals
    in_progress_call = call_inference_activity_on_chunk(chunk)
    append in_progress_call to array_of_tasks

collected_responses = await array_of_tasks
summarised_response = aggregate_responses(collected_responses)

return summarised_response

```

By performing the individual sequence processing within separate activity functions, we can leverage the parallelism and fault tolerance of Durable Function apps. In the event that one of the individual executions fails, that individual activity is restarted, rather than the entire orchestration.

Each of these individual activity function executions communicate (over HTTPS) with a Kubernetes-backed model endpoint, deployed via the Azure Machine Learning (AML) service. These connections are internally routed through an AML-created load balancer pod layer, to the model endpoints where inference is then performed (both hosted within the Azure Kubernetes Service).

This enables a level of elasticity within the system: model endpoints can be created and destroyed dynamically, and a system "state" can be maintained, where state can be seen as the number of active endpoints (currently performing inference) and readied endpoints (endpoints that are available for inbound connections but idle). This state is maintained via two "levers": internally to Kubernetes, where extra model replica pods are created when there is additional load into the system, and at an infrastructure level, where extra nodes (virtual machines) can be allocated to Kubernetes, thus leading to capacity of:

$$\text{available endpoints} \approx \text{node pool count} * \left(\frac{\text{total node resources}}{\text{single instance utilisation}} \right)$$

As such, we have multiple levers by which we can dynamically adjust the system in response to demand (either dynamically via AKS, or vertically by adjusting node pool specification for higher/lower SKU machines). This level of flexibility is required for multiple reasons. First, because the system is going to be under variable load over a 24 hour period as a result of requests coming directly from cardiologists, and thus would be cost-inefficient if it was unable to flexibly allocate and deallocate resources. Second, because the endpoints are receiving a single short segment of a larger signal, load through to the model endpoints is also dependent on signal length. For instance, a two minute ECG signal, separated into 8 second sequences with 1 second of overlap leads to 17+ separate model endpoint calls (allowing for call failures and retries). Signals are not of uniform length, and so the number of calls will rise and fall dependent on their duration.

6.1 MLOps and Integration

"MLOps" refers to a loosely associated set of principles, partially derived from "DevOps", specific to the domain of machine learning systems. As a result, there is no universally-agreed set of features that an "MLOps-guided" system should exhibit, but we have placed importance upon the following principles:

- Results of model training runs, model weight versions should be "indefinitely stored" with the ability to deploy and redeploy inference components with newer or older versions of model weights.
- Deployment of system components should be automated, without the need for a person to manually deploy or configure individual services.
- The system should be "transparent", where any individual component can be monitored with low effort.

- Deployment of the system and configuration of the components should ultimately be stored and executed via code, rather than front-end or UI components.
- There should be no doubt that the system will operate as expected in the production environment. Conversely, it should be impossible to deploy a version of the system where certain behaviours are not guaranteed.

With these principles in mind, the need for a thorough DevOps/MLOps arrangement was made clear. This arrangement was enabled via Azure DevOps (ADO) and the Azure Machine Learning service; primarily orchestrated via Git commit and pull triggers. As the models are deployed on a microservice architecture, we're able to individually update and configure components without redeploying or altering adjacent components (barring API changes). Via ADO build and release pipelines, these changes can also be sequentially deployed through DEV, QA and PROD environments, to reduce the chance of unexpected errors when they arrive in PROD.

- **Merge to main of middleware code.** Triggers a pipeline where middleware changes are sequentially deployed and tested across environments.
- **Merge to main of model training code.** Triggers a pipeline where a new batch AML endpoint for the model training is sequentially deployed, a training run is initiated, and a new model artifact is produced along with error metrics.
- **New version of the model weights registered to Azure Machine Learning model registry.** Leads to an evaluation of whether the new model is of comparable performance. If they are, the inference webservice are updated with the new model.
- **Merge to main of inference code.** Triggers a pipeline where the new inference code is sequentially deployed and tested across environments.

Following these controls, we're able to maintain the system on a service-by-service basis, while being able to effectively manage the complexity of the overall interactions. Monitoring of the individual components was enabled by Azure Application Insights, which integrates with Azure Functions and AML-backed Kubernetes deployments, and yields telemetry such as application logs, response times, and individual node statuses.

7 Discussion

7.1 Model Performance

Our experimental results demonstrate that a deep neural network architecture can render solid results in detection of normal vs abnormal ECG records for canines, and most of the time perform on par with trained cardiologists. Furthermore, we saw that the continuous wavelet approach associated to the augmentation paradigm allows to handle the signal data as an image and then to leverage classical deep learning technics. In particular, it seems that our custom models are performing slightly better comparatively to pre-trained resnet models.

Last but not least, the deployment of the solution in the cloud with the activation of MLOps features makes the entire solution more flexible, reliable and scalable.

7.2 Application and Future Work

Cardiac arrhythmias are associated with an increased risk of sudden death in dogs[40][41]. Cardiac arrhythmias can be found in dogs who are considered healthy, indicating a need for increased screening [42][43]. However, diagnosis of canine arrhythmias is a challenge for many veterinarians, due to a combination of factors [44]. Cited issues include lack of access to ECG monitoring capability or lack of training in ECG interpretation. Automated tools such as the one developed in this work can improve decision support and enhance quality of care available to pets. Normal vs abnormal classification provides a valuable first step to automated ECG diagnosis of individual rhythms. Different cardiac arrhythmias and underlying cardiac pathologies require individualized treatment [15]. For this reason future work will focus on multi-label diagnosis of ECG abnormalities including arrhythmias. Prediction

of specific arrhythmias and abnormalities will allow veterinarians to make more complex decisions in real-time including referral to cardiology specialist.

8 References

References

- [1] Pierre Menaut, Marie C Bélanger, Guy Beauchamp, Nicole M Ponzio, and N Sydney Moïse. Atrial fibrillation in dogs with and without structural or functional cardiac disease: a retrospective study of 109 cases. *Journal of Veterinary Cardiology*, 7(2):75–83, 2005.
- [2] ARM Gelzer, MS Kraus, M Rishniw, NS Moïse, R Pariaut, SA Jesty, and SA Hemsley. Combination therapy with digoxin and diltiazem controls ventricular rate in chronic atrial fibrillation in dogs better than digoxin or diltiazem monotherapy: a randomized crossover study in 18 dogs. *Journal of veterinary internal medicine*, 23(3):499–508, 2009.
- [3] RA Santilli, M Perego, A Perini, P Moretti, and G Spadacini. Electrophysiologic characteristics and topographic distribution of focal atrial tachycardias in dogs. *Journal of Veterinary Internal Medicine*, 24(3):539–545, 2010.
- [4] M Perego, L Ramera, and RA Santilli. Isorhythmic atrioventricular dissociation in labrador retrievers. *Journal of veterinary internal medicine*, 26(2):320–325, 2012.
- [5] RA Santilli, M Mateos Pañero, DM Porteiro Vázquez, A Perini, and M Perego. Radiofrequency catheter ablation of accessory pathways in the dog: the italian experience (2008–2016). *Journal of Veterinary Cardiology*, 20(5):384–397, 2018.
- [6] Roberto A Santilli, Luis FN Santos, and Manuela Perego. Permanent junctional reciprocating tachycardia in a dog. *Journal of Veterinary Cardiology*, 15(3):225–230, 2013.
- [7] Roberto A Santilli, Manuela Perego, Alberto Perini, Andrea Carli, Paolo Moretti, and Gianmario Spadacini. Radiofrequency catheter ablation of cavo-tricuspid isthmus as treatment of atrial flutter in two dogs. *Journal of Veterinary Cardiology*, 12(1):59–66, 2010.
- [8] Roberto A Santilli, Lucia Ramera, Manuela Perego, Paolo Moretti, and Giammario Spadacini. Radiofrequency catheter ablation of atypical atrial flutter in dogs. *Journal of Veterinary Cardiology*, 16(1):9–17, 2014.
- [9] S Battaia, M Perego, and R Santilli. Radiofrequency catheter ablation of cranial vena cava flutter in four dogs. *Journal of Veterinary Cardiology*, 36:123–130, 2021.
- [10] RA Santilli, LV Bontempi, and M Perego. Ventricular tachycardia in english bulldogs with localised right ventricular outflow tract enlargement. *Journal of Small Animal Practice*, 52(11):574–580, 2011.
- [11] M Mateos Pañero, S Battaia, L Ramera, M Perego, and RA Santilli. R-peak time in clinically healthy dogs with different thoracic conformations. *The Veterinary Journal*, 268:105592, 2021.
- [12] Eva M Oxford, Flavia B Giacomazzi, N Sydney Moïse, and Roberto A Santilli. Clinical and electrocardiographic presentations of transient trifascicular block in three cats. *Journal of Veterinary Cardiology*, 20(3):204–212, 2018.
- [13] S Battaia, M Perego, C Perciballi, D Cavallini, and R Santilli. Noninvasive electrocardiographic parameters to assess interventricular dyssynchrony in dogs with bundle branch blocks. *Journal of Veterinary Cardiology*, 41:134–144, 2022.
- [14] Lisa Wogan. Specialist shortage opens door to larger industry role in training, Apr 2022. URL <https://news.vin.com/default.aspx?pid=210&Id=10904281&f5=1>.
- [15] Roberto Santilli, Sydney Moïse, Romain Pariaut, and Manuela Perego. Electrocardiography of the dog and cat.: Diagnosis of arrhythmias. Edra, 2019.

- [16] Roberto A Santilli, Dolores Maria Porteiro Vázquez, Magda Gerou-Ferriani, Sergio F Lombardo, and Manuela Perego. Development and assessment of a novel precordial lead system for accurate detection of right atrial and ventricular depolarization in dogs with various thoracic conformations. *American Journal of Veterinary Research*, 80(4):358–368, 2019.
- [17] U Rajendra Acharya, Shu Lih Oh, Yuki Hagiwara, Jen Hong Tan, and Hojjat Adeli. Deep convolutional neural network for the automated detection and diagnosis of seizure using eeg signals. *Computers in biology and medicine*, 100:270–278, 2018.
- [18] Awni Y Hannun, Pranav Rajpurkar, Masoumeh Haghpanahi, Geoffrey H Tison, Codie Bourn, Mintu P Turakhia, and Andrew Y Ng. Cardiologist-level arrhythmia detection and classification in ambulatory electrocardiograms using a deep neural network. *Nature medicine*, 25(1):65–69, 2019.
- [19] Özal Yildirim, Paweł Pławiak, Ru-San Tan, and U Rajendra Acharya. Arrhythmia detection using deep convolutional neural network with long duration ecg signals. *Computers in biology and medicine*, 102:411–420, 2018.
- [20] AH Estrada, A Spake, ME Kleman, D Leeder, D Blischok-Lapekas, M Margiocco, J Gentile-Solomon, N Piscitelli, and D Szlosek. Diagnostic accuracy of computer aided electrocardiogram analysis in dogs. *Journal of Small Animal Practice*, 62(2):145–149, 2021.
- [21] Mohammad Kachuee, Shayan Fazeli, and Majid Sarrafzadeh. Ecg heartbeat classification: A deep transferable representation. In *2018 IEEE international conference on healthcare informatics (ICHI)*, pages 443–444. IEEE, 2018.
- [22] Gari D Clifford, Chengyu Liu, Benjamin Moody, H Lehman Li-wei, Ikaro Silva, Qiao Li, AE Johnson, and Roger G Mark. Af classification from a short single lead ecg recording: The physionet/-computing in cardiology challenge 2017. In *2017 Computing in Cardiology (CinC)*, pages 1–4. IEEE, 2017.
- [23] Glenn Van Steenkiste, Gunther van Loon, and Guillaume Crevecoeur. Transfer learning in ecg classification from human to horse using a novel parallel neural network architecture. *Scientific Reports*, 10(1):186, 2020.
- [24] Ying Liao, Yisha Xiang, Mingjie Zheng, and Jun Wang. Deepmicetl: a deep transfer learning based prediction of mice cardiac conduction diseases using early electrocardiograms. *Briefings in Bioinformatics*, page bbad109, 2023.
- [25] Nathan M Thomas. *ECG classification of canine arrhythmias using deep neural networks*. PhD thesis, 2021.
- [26] Matthew A Reyna, Nadi Sadr, Erick A Perez Alday, Annie Gu, Amit J Shah, Chad Robichaux, Ali Bahrami Rad, Andoni Elola, Salman Seyedi, Sardar Ansari, et al. Will two do? varying dimensions in electrocardiography: the physionet/computing in cardiology challenge 2021. In *2021 Computing in Cardiology (CinC)*, volume 48, pages 1–4. IEEE, 2021.
- [27] Connor Shorten and Taghi M Khoshgoftaar. A survey on image data augmentation for deep learning. *Journal of big data*, 6(1):1–48, 2019.
- [28] Naoki Nonaka and Jun Seita. Randecg: Data augmentation for deep neural network based ecg classification. In *Advances in Artificial Intelligence: Selected Papers from the Annual Conference of Japanese Society of Artificial Intelligence (JSAI 2021)*, pages 178–189. Springer, 2022.
- [29] M Jorge Cardoso, Wenqi Li, Richard Brown, Nic Ma, Eric Kerfoot, Yiheng Wang, Benjamin Murrey, Andriy Myronenko, Can Zhao, Dong Yang, et al. Monai: An open-source framework for deep learning in healthcare. *arXiv preprint arXiv:2211.02701*, 2022.
- [30] Ekin D Cubuk, Barret Zoph, Jonathon Shlens, and Quoc V Le. Randaugment: Practical automated data augmentation with a reduced search space. In *Proceedings of the IEEE/CVF conference on computer vision and pattern recognition workshops*, pages 702–703, 2020.

- [31] Amara Graps. An introduction to wavelets. *IEEE computational science and engineering*, 2(2): 50–61, 1995.
- [32] Paul S Addison. Wavelet transforms and the eeg: a review. *Physiological measurement*, 26(5): R155, 2005.
- [33] Thomas H Cormen, Charles E Leiserson, Ronald L Rivest, and Clifford Stein. *Introduction to algorithms*. MIT press, 2022.
- [34] Kaiming He, Xiangyu Zhang, Shaoqing Ren, and Jian Sun. Deep residual learning for image recognition. In *Proceedings of the IEEE conference on computer vision and pattern recognition*, pages 770–778, 2016.
- [35] Hossein Gholamalinezhad and Hossein Khosravi. Pooling methods in deep neural networks, a review. *arXiv preprint arXiv:2009.07485*, 2020.
- [36] William A Falcon. Pytorch lightning. *GitHub*, 3, 2019.
- [37] Xavier Glorot and Yoshua Bengio. Understanding the difficulty of training deep feedforward neural networks. In *Proceedings of the thirteenth international conference on artificial intelligence and statistics*, pages 249–256. JMLR Workshop and Conference Proceedings, 2010.
- [38] Zhilu Zhang and Mert Sabuncu. Generalized cross entropy loss for training deep neural networks with noisy labels. *Advances in neural information processing systems*, 31, 2018.
- [39] Zhaoqi Leng, Mingxing Tan, Chenxi Liu, Ekin Dogus Cubuk, Xiaojie Shi, Shuyang Cheng, and Dragomir Anguelov. Polyloss: A polynomial expansion perspective of classification loss functions. *arXiv preprint arXiv:2204.12511*, 2022.
- [40] R Santilli, V Saponaro, L Carlucci, M Perego, S Battaia, and M Borgarelli. Heart rhythm characterization during sudden cardiac death in dogs. *Journal of Veterinary Cardiology*, 38:18–30, 2021.
- [41] Kieran Borgeat, Matthew Pack, Jo Harris, Alex Laver, Joonbum Seo, Omri Belachsen, Joshua Hannabuss, Julie Todd, Luca Ferasin, and Jessie Rose Payne. Prevalence of sudden cardiac death in dogs with atrial fibrillation. *Journal of Veterinary Internal Medicine*, 35(6):2588–2595, 2021.
- [42] Felix M Duerr, Anthony P Carr, Tanya Duke, Cindy L Shmon, and Eric Monnet. Prevalence of perioperative arrhythmias in 50 young, healthy dogs. *The Canadian Veterinary Journal*, 48(2): 169, 2007.
- [43] Solimar Dutra Silveira, Bruna Gabriela Gheller, and Andréa Christina Ferreira Meirelles. Pre-operative electrocardiographic study of dogs at the veterinary hospital of pontificia universidade católica do paraná. *Ciência Animal Brasileira*, 19, 2018.
- [44] Arnaut Hellemans, Mark Schittekatte, Marc Covents, and Pascale Smets. Diagnosis and management of arrhythmias in dogs: A cross-sectional online survey among flemish veterinary practitioners. *Veterinary Record Open*, 9(1):e35, 2022.